

# Unveiling midcrustal seismic activity at the front of the Bolivian altiplano, Cochabamba region

G.A. Fernandez <sup>\*1</sup>, B. Derode <sup>2,3,5</sup>, L. Bollinger <sup>3</sup>, B. Delouis <sup>4</sup>, M. Nieto <sup>1</sup>, F. Condori <sup>1</sup>, N. Sarret<sup>1</sup>, J. Letort <sup>5</sup>, S. Godey <sup>3</sup>, M. Wimez <sup>1</sup>, T. Griffiths <sup>1</sup>, W. Arce <sup>1</sup>

<sup>1</sup>Observatorio San Calixto, La Paz, Bolivia, <sup>2</sup>EOST, ITES, CNRS UMR 7063, Université de Strasbourg, Strasbourg, France, <sup>3</sup>CEA, DIF, F-91297, Arpajon, France, <sup>4</sup>Géoazur, CNRS UMR 7329, Université Côte d'Azur, France, <sup>5</sup>Observatoire Midi Pyrénées, IRAP, CNRS UMR 5277, Université Paul Sabatier, Toulouse, France

**Author contributions:** *Conceptualization, data curation, investigation, methodology, software and visualization:* G.A. Fernandez, B. Derode, L. Bollinger, B. Delouis, J. Letort, M. Wimez.. *Formal analysis:* G.A. Fernandez, B. Derode, L. Bollinger, B. Delouis, M. Nieto, F. Condori, N. Sarret, J. Letort, S. Godey, M. Wimez, T. Griffiths, W. Arce.. *Funding acquisition:* L. Bollinger and B. Delouis.. *Supervision:* G.A. Fernandez, B. Derode, L. Bollinger, B. Delouis.. *Writing and review process:* G.A. Fernandez, B. Derode, L. Bollinger, B. Delouis, M. Nieto.

**Abstract** Located in the heart of the Bolivian orocline, the Cochabamba department and its two million inhabitants are exposed to frequent seismic activity. However, the tectonic structures causing these earthquakes remain poorly identified. Indeed, Bolivia's national seismological network does not optimally cover the area and the hypocentral locations of local earthquakes are therefore associated to large uncertainties, which hinder their association with specific faults. We established a regional network consisting of 11 broadband and short-period seismic stations, spaced approximately 20 km apart. This study highlights the initial 6-month seismic report, which involved an automated deep neural network-based seismic phase picking utilizing a pre-trained model. A thorough comparison with a manual catalog by seismic analysts is conducted for validation. Focal mechanisms of significant earthquakes are determined from full waveform inversion and polarities. The seismic activity appears to be concentrated in the Main Thrust fault shear zone, and in its hanging wall, a stack of tectonic slivers affected by transverse faults. The depth of the events beneath the network is shallower than was previously thought. Seismic clusters in the Main Thrust System below the toe of the high topography are likely caused by strain and stress build-up on the frontal decollement. These results therefore provide new insights and hypotheses into the seismogenic behavior and potential of the fault system across the Bolivian orocline.

**Non-technical summary** The intraplate seismic events in Bolivia predominantly occur in the central part of the country. However, a comprehensive study of these earthquakes is still lacking due to the limited availability of seismic stations and geological studies, among others. This dearth of information makes it challenging to correlate these seismic events with specific geological fault systems. Consequently, conducting seismic hazard assessments in this region remains a formidable task, but necessary given the exposure of the 2 million inhabitants population. The present study aims to address this gap by providing valuable insights into the seismic activity of the area to improve understanding of shallow seismic events and the potential for significant earthquakes.

## 1 Introduction

The Andes mountain range is a prominent geological feature on Earth formed by the subduction of the Nazca oceanic plate beneath the South American continent. The system currently experiences a shortening rate of approximately 7 to 8 cm/yr (e.g., Jarrin et al., 2022; Pardo-Casas and Molnar, 1987). While the majority of the shortening is absorbed at the Nazca trench, about 1 cm/yr of shortening is transmitted eastward and absorbed by continental subduction of the Brazilian (BS) shield beneath the Eastern Cordillera (EC), as illustrated in Figure 1 (e.g., Brooks et al., 2011; Isacks, 1988; Mercier et al., 1992; Weiss et al., 2016). These geodynamic conditions result in frequent earthquakes, some

of them large and devastating, well documented historically and instrumentally along the oceanic subduction trough (e.g., Beck et al., 1998; Campos et al., 2002; Devlin et al., 2012; Madariaga et al., 2010; Sempere et al., 1990; Vega and Buforn, 1991; Ruiz et al., 2016). In contrast, a few intermediate and strong earthquakes ( $M > 6$ ) occur along the eastern edge of the Altiplano (AP) beneath the Eastern Cordillera (EC), InterAndean (IA) and SubAndean (SA) (e.g., Fernandez et al., 2019; Funning et al., 2005; Rivadeneyra-Vera et al., 2016).

The Observatorio San Calixto (OSC) has been monitoring this seismic activity using Bolivia's national seismic network (RS-OSC) since 1913. The network currently consists of 13 permanent seismic stations and 3 strong-motion sensors. These seismic stations are reported on Figure 1 (Nieto et al., 2021).

\*Corresponding author: tonino.gafm@gmail.com

Production Editor:  
Carmine Galasso  
Handling Editor:  
Andrea Llenos  
Copy & Layout Editor:  
Théa Ragon

Received:  
May 16, 2024  
Accepted:  
January 6, 2025  
Published:  
January 29, 2025

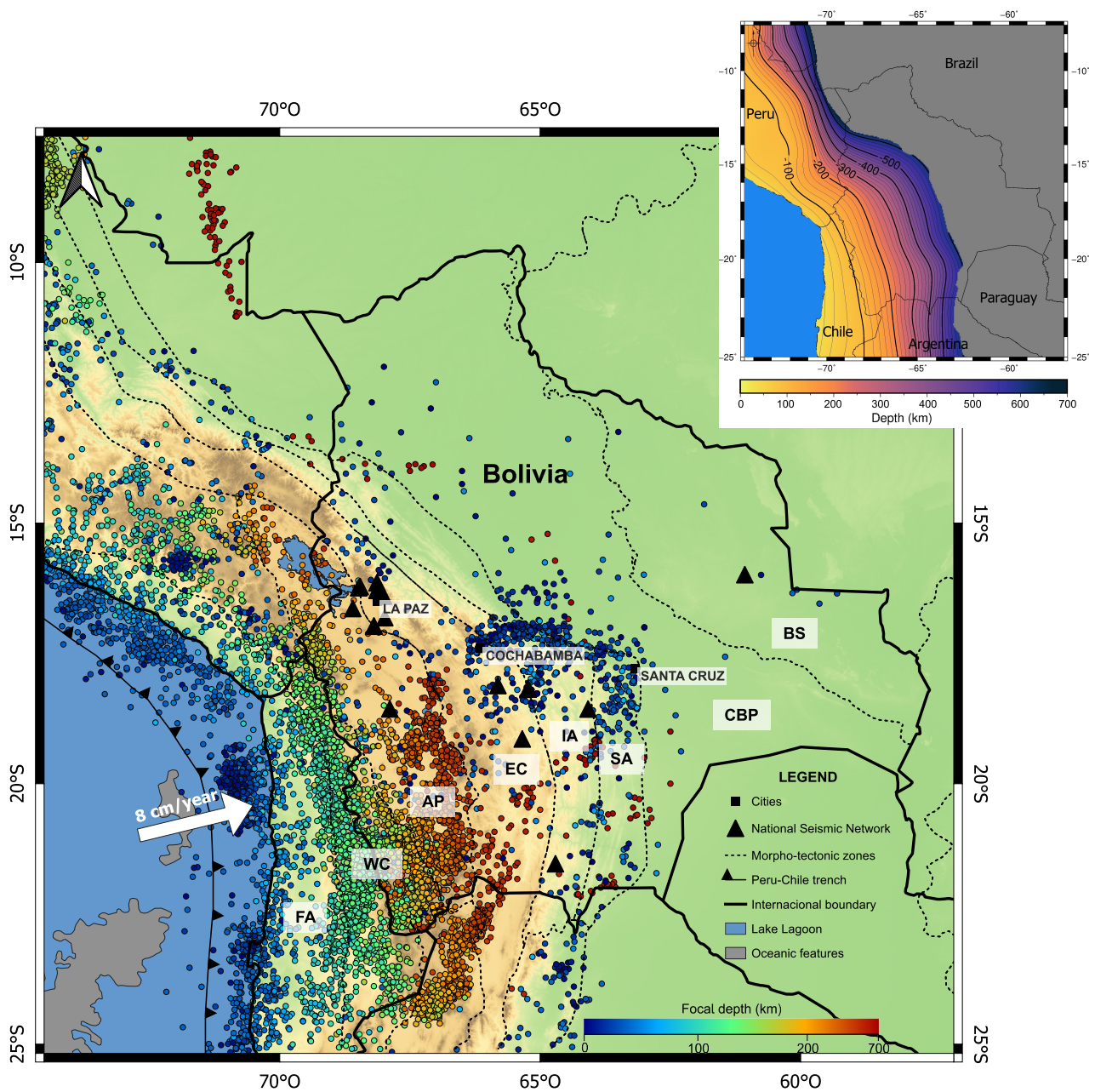


**Figure 1** Distribution of seismic activity in the central part of the Central Andes (Bolivia), Observatorio San Calixto seismic catalog from 1913 to 2021. Depth of the earthquakes (circles) are indicated by the colored scale. Black triangles represent the national seismic network operated by the OSC. The white arrow shows the motion of the oceanic Nazca plate with respect to South America, with the associated value of convergence. The depths of the subducting slab (Slab2, Hayes et al., 2018) modeled in the region are illustrated on the upper right panel.

Seismic activity recorded by the OSC to the west of the Bolivian territory beneath the Western Cordillera (WC) is mainly associated with the subduction of the Nazca plate beneath the South American plate. Earthquakes occur here at depths ranging from 0 to 200 km. A deeper seismic activity, still connected to the subduction process, is observed beneath the AP zone (Figure 1), extending further eastward below the EC zone and Chaco Basin Plains (CBP) zones, with depths occasionally exceeding 500 km (e.g., Jimenez et al., 2014; Lavenu, 2006; Silver et al., 1995; Zhan et al., 2014). Shallower seismic activity is concentrated along the eastern margin of the AP Zone, from the EC Zone to the front of the mountain

range. Most of this historical and instrumental seismic activity has been located in the center of the Bolivian Orocline (BO).

The Bolivian Orocline (BO) is segmented and made of two main limbs: a Northern limb that trends northwest-southeast and a Southern limb that trends north-south. The axis of the bending is located within the Cochabamba department. Various studies have identified a complex active fault system in the area, including normal fault segments bounding the Cochabamba, Sacaba and Punata basins and the active strike slip fault systems of the Tunari-Cochabamba Fault (CF) and the Rio Novillero Fault (RNF) (Baby et al., 1992; Eichel-

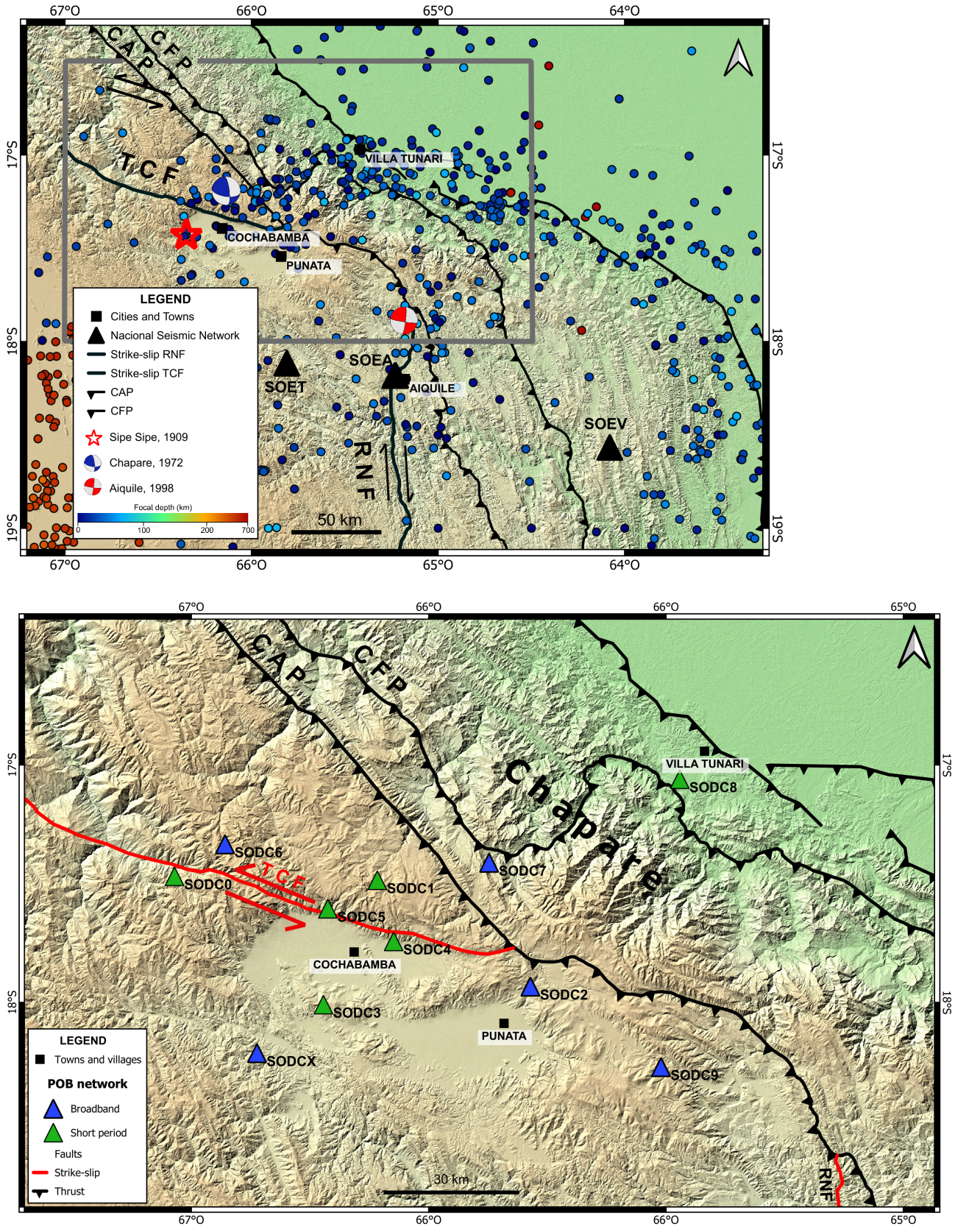


**Figure 2** (Top) Distribution of shallow earthquakes 1990-2022 within the central region of the Bolivian Orocline recorded by the permanent national seismic network (black triangles). Two geological fault systems, namely the Cochabamba Fault (TCF) and the Rio Novillero Fault (RNF), are indicated with double black arrows showing their sense of motion. CAP and CFP respectively for Main Andean Thrust and Main Frontal Thrust. (Bottom) Location of the stations of the temporary seismic network. Green and blue triangles stand respectively for short-period (Sercel L22) and broadband seismic stations (Trillium 120 and Guralp 6 TD).

berger and McQuarrie, 2015; Funning et al., 2005; Kley, 1999; Lamb, 2000; Weiss et al., 2016).

Significant seismic events have been documented within the region. The latest destructive earthquake occurred near Aiquile at about 100 km to the south of Cochabamba on May 22, 1998 (Figure 2a). This destructive Mw 6.6 shallow earthquake activated the right-lateral Rio Novillero fault (Funning et al., 2005), attesting for the high seismogenic potential of the secondary faults in the area. Other destructive earthquakes, less documented, happened also within or in the vicinity of the Cochabamba basin, on May 12, 1972 in Cochabamba, as well as on July 23, 1909 in Sipe Sipe, 20 km west of the city center (Vega, 1996). In addition to these earthquakes, every year, the national network records a few dozen local earthquakes ( $M > 3.0$ ), the location of which is subjected to a large uncertainty - sometimes more than a dozen kilometres - and which therefore cannot be directly associated with any particular segment of the fault systems. The hypocentral depth of these earthquakes remains poorly constrained (due to the scattered seismic stations in Bolivia). This limits the capacity to associate a seismogenic potential to the faults responsible for the regional seismic hazard.

This study introduces the Proyecto Oroclino Boliviano Network (POBnet), which is the first earthquake monitoring system in the central region of the Bolivian orocline, encompassing the Cochabamba, Punata, Sacaba, and Chapare regions (Figure 2b). The network, established in 2022, comprises 11 seismic stations. Its principal objectives are to enhance the local earthquake detection capacity, improve the accuracy of earthquake location, determine new focal mechanisms, and associate earthquakes to the fault system surveyed by geologists. This study describes an "automated workflow" using a supervised Deep Neural Network (DNN) approach called PhaseNet (Zhu and Beroza, 2018) and a manual "analyst workflow" led by expert seismologists in order to estimate and to validate the capacity of the automated workflow. This study examines the effect of the velocity model on the earthquake locations and also explores the potential of moment tensor inversion for moderate to small earthquakes (Mw 2.5 and 4.1). Finally, it compares the earthquake catalog with a geological balanced cross-section in order to draw seismotectonic implications.

## 2 Methodology

### 2.1 Network Deployment

The POBnet seismic network was deployed and became operational in April 2022. It consists of 6 Sercel-L22 short period instruments, 4 Trillium-compact-120s broadband instruments, and 1 Güralp 6TD-30s medium band instrument. The 32-bit digitizers (STANEO DDB6-Mob and Güralp-EAM) operate at a rate of 100 samples per second, and all instruments are synchronized by GPS (Table S1). The distribution of POB seismic stations is shown in Figure 2b.

To understand the anthropogenic noise behavior at each seismic station and ensure the data's suitability for

this research, we performed probabilistic power spectral density computations to assess the potential impact of cultural noise on our data, following McNamara (2004). Our results indicate that the noise spectra are closer to the low noise model than the high noise of Peterson (1993) for most stations, while a few specific stations - deployed in the vicinity of the cities - are exposed to cultural noise and show more intermediate signatures (Figure S1 presents one short period and one broadband data examples).

### 2.2 Workflow

For the purposes of this study, a workflow has been developed that combines manual picking and fully automated deep-learning methods followed by quality control approaches (see Figure S2). The aim of this approach is to make the most of the temporary network's efficiency in detecting and locating small earthquakes in the study area, while also ensuring the homogeneity and accuracy of the phase picking process (Savvaidis et al., 2019; Walter et al., 2019). This is a crucial step in obtaining valuable seismic locations, even for small earthquakes ( $M_L < 3.5$ ).

The workflow used in this study is illustrated in Figure 3. Seismic waveforms are manually processed through Seisan for P and S phase picking, phase association, amplitude measurements, and hypocentral locations with Hypo71 (Havskov et al., 2020; Lee and Lahr, 1975). Simultaneously, the automatic detection of earthquakes on the continuous miniseed files and the seismic phase picking process is done with the deep learning-based method PhaseNet (Zhu and Beroza, 2018). The P and S picks are then associated and located with REAL - the Rapid Earthquake Association and Location algorithm (Zhang et al., 2019).

Analysts at OSC then compare the automated catalog with the manual catalog to ensure that no events are missing from the automated catalog. They also review the signals associated with the events detected by the automated workflow to avoid false positive detections and to check the quality of the phase picks.

### 2.3 Automatic Phase Picking and Association

The PhaseNet picking method (Zhu and Beroza, 2018) is an entirely automated approach consisting of a supervised deep neural network (DNN), trained on a dataset of nearly 800,000 three-component recordings from the Northern California Earthquake Data Center (NCEDC, 2014). This method identifies and picks the regional P and S wave arrivals automatically from three-component 30(s) windowed seismic signals.

PhaseNet has been used successfully for the detection and identification of seismic phase arrivals in a variety of seismic environments including volcanic settings and mountain belts (e.g., Ammirati et al., 2022; Derode et al., 2023; Retailleau et al., 2023).

In this study, we applied the PhaseNet probabilities thresholds of 0.5 and 0.55 for P and S wave arrivals. These thresholds are intentionally set high (compare to the 0.3 threshold now currently use to ensure a better

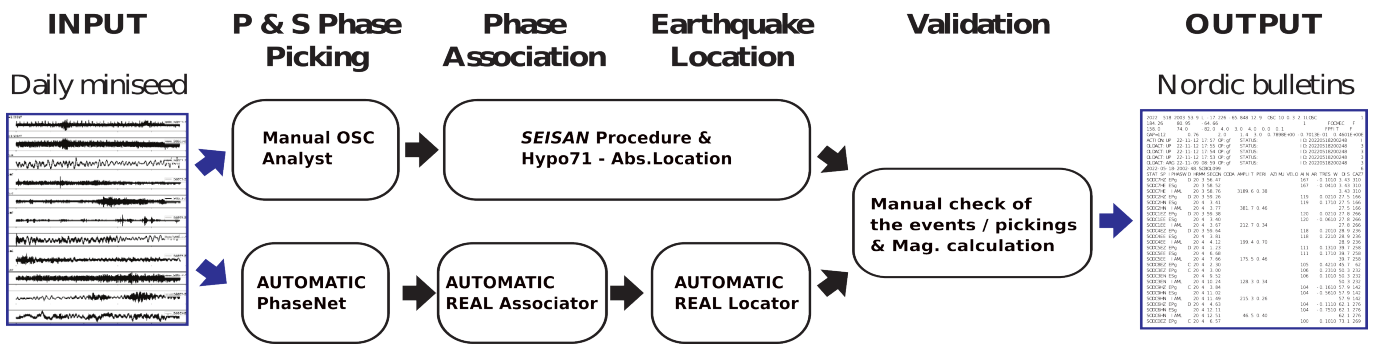


**Figure 3** Sketch of the global workflow used to detect and pick seismic phases using both manual and automatic algorithms. Results are merged in a seismic bulletin after being validated by the analysts of the OSC.

recall) to guarantee, after association and location processes, high precision, recall and F1-score (e.g., Glasgow et al., 2021; Jiang et al., 2021; Tan et al., 2021; Zhang et al., 2022). Table S2 presents the computation of Precision, Recall and F1 metrics.

Despite the availability of new seismic phase association algorithms, such as GENIE (McBrearty and Beroza, 2023) or GAMMA (Zhu et al., 2022), we have chosen to use the REAL algorithm (Zhang et al., 2019). In fact, this algorithm, which has been accessible to the public for over four years, has been subjected to rigorous testing in a multitude of studies (e.g., Ammirati et al., 2022; Derode et al., 2023), thereby substantiating its potential and reliability for the specific instrumental network in question. REAL combines the advantages of pick-based and waveform-based detection and location methods. Unlike waveform-based methods that use continuous seismic data to search for events in 3D space, REAL focuses on a smaller area around the station with the current initiating phase and seismic picks. We used a coarse grid (0.02° x 0.02° x 2 km) to generate travel time tables for each source station pair, based on the Ryan et al. (2016) velocity model (Table S3a).

In order to ensure a good quality of the detected events based on the multiple picks of the PhaseNet detections, we imposed a minimum of 4 P and 2 S on 4 different stations to consider an event detection. Then 6 phases (with PhaseNet probabilities higher than 0.5) on 4 different stations are needed to associate and prelocate an event with REAL. We then use the Hypo71 routines (Lee and Lahr, 1975) to obtain the absolute earthquake location.

### 2.4 Velocity Model

The 1D velocity model extracted for the Cochabamba region from Ryan et al. (2016) exhibits comparable Vp and Vs velocities to those documented in the literature for the eastern front of the Andes in northwestern Argentina (e.g., Ammirati et al., 2015; Venerdini et al., 2020). The regional velocity model derived from the receiver function study by Ryan et al. (2016) suggests that the velocity model covering the Altiplano to Brazilian craton is more likely to be 2D in relation to the geological anisotropy found in the area. The use of a 1D model could result in the biasing of earthquake locations. This is to be expected at a large scale, but could also be sen-

sitive at the smaller scale of our network.

Two approaches were considered in order to validate the velocity model proposed.

1. Vp/Vs derived from Wadati plot: The Wadati diagrams were determined for each seismic station (Figure S3). The Vp/Vs ratio estimated from this diagram is then compared with the Vp/Vs ratios determined by Ryan et al. (2016). We then assessed the potential impact of the local Vp/Vs on the seismic locations.
2. A joint relocation and inversion of the 1D velocity model was conducted. We used the joint hypocenter, velocity model, and station coefficient determination using VELEST (Kissling et al., 1994) and the Joint Hypocenter Determination method (Pujol, 1992). In order to conduct this analysis, a set of relatively well-constrained earthquakes was selected from the initial catalog, comprising approximately 439 mid-crustal events. These events were then tested against the velocity model proposed by Ryan et al. (2016) in order to evaluate any discrepancies and refine the parameters of our model.

### 2.5 Focal Mechanism from Near source seismological records (FMNEAR)

The FMNEAR method was first introduced in Delouis (2014). Full waveforms in displacement at local to regional distance are inverted using a non linear approach combining a grid search and simulated annealing. The option to invert P-wave polarities in conjunction with the waveforms has been recently added and may be especially helpful to constrain the solution of small earthquakes (M < 3). The parameters to be determined are the strike, dip, rake parameters of the double couple focal mechanism, the moment rate source time function, hence the seismic moment and the moment magnitude Mw, and the source depth.

Pre-processing steps include trend and offset removal, integration of the broadband records, deconvolution of the short period records by their instrumental response, P-wave manual picking with polarity information. Synthetic seismograms are computed by the wavenumber integration method of Bouchon (1981) adopting a 1D velocity model based on Ryan et al. (2016) (Table S3a). The user can adjust the filtering band for

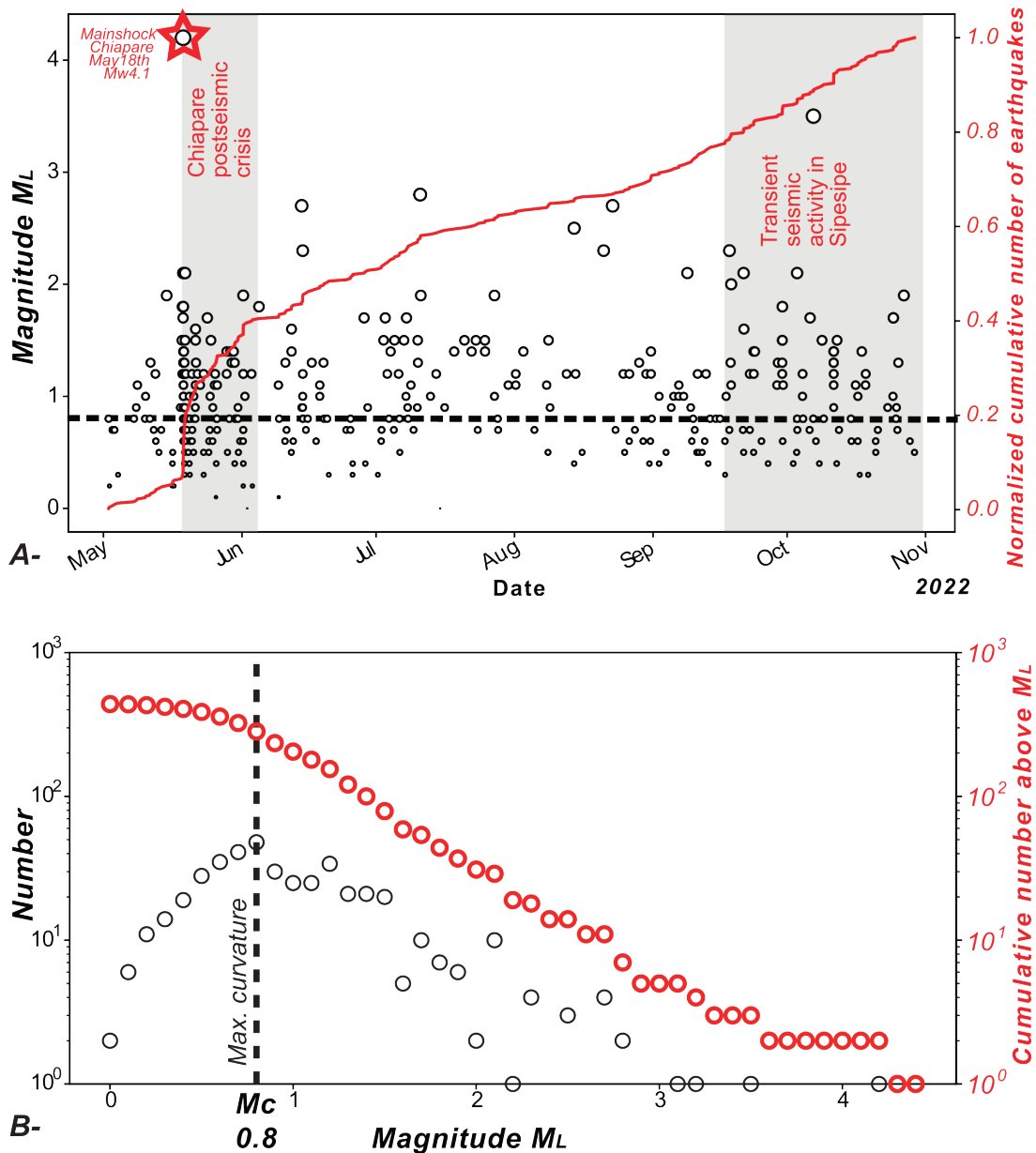


**Figure 4** (a) Scatter plot of the magnitude of the earthquakes recorded from May to end of October 2022 in the region of interest. Gray shaded areas delimitate the period of the two seismic clusters in Chapare and Sipesipe zones, the black dashed line indicates the completeness magnitude ( $M_c$ ), and the red solid line represents the cumulative number of earthquakes in the automatic catalogue. (b) Frequency – Magnitude Distribution for the automatic seismic catalog, the light blue dashed line is the  $M_c$  value computed by the Maximum Curvature Method (MAXC), white dots are the number of events per bin and red dots represents the cumulative value.

each station and component individually and explore source depth with a user-defined depth step.

### 3 Results

#### 3.1 Detection and location

The main results from the first six months of seismic monitoring in the Cochabamba region indicate the presence of an intense microseismic activity below the network. Specifically, 439 earthquakes associated with magnitudes greater than  $M_L$  0.2 were detected during this period (Figure 4a). The completeness magnitude  $M_c$  of the automatic catalog is estimated to be approximately  $M_L$  0.83 using the Maximum Curvature Method,

also known as MAXC, (Figure 4b), indicating the network’s capability to detect and locate very small earthquakes within the region (Wiemer and Wyss, 2000).

In order to evaluate the precision of the picks obtained through our procedure, we conducted a comparison between the outcomes from manual and PhaseNet techniques across the entire dataset. This entailed the calculation of time differences between the analysts’ and the automatic picks. The methods yielded comparable arrival times for P and S, with standard deviations of the differences lower than 0.26 seconds (0.20s and 0.26s for P and S waves, respectively, Figure 5c-e). Considering a theoretical maximum P velocity of 6 km/s, these statistical differences should not involve earthquake location differences higher than 1.5-2 km. This is

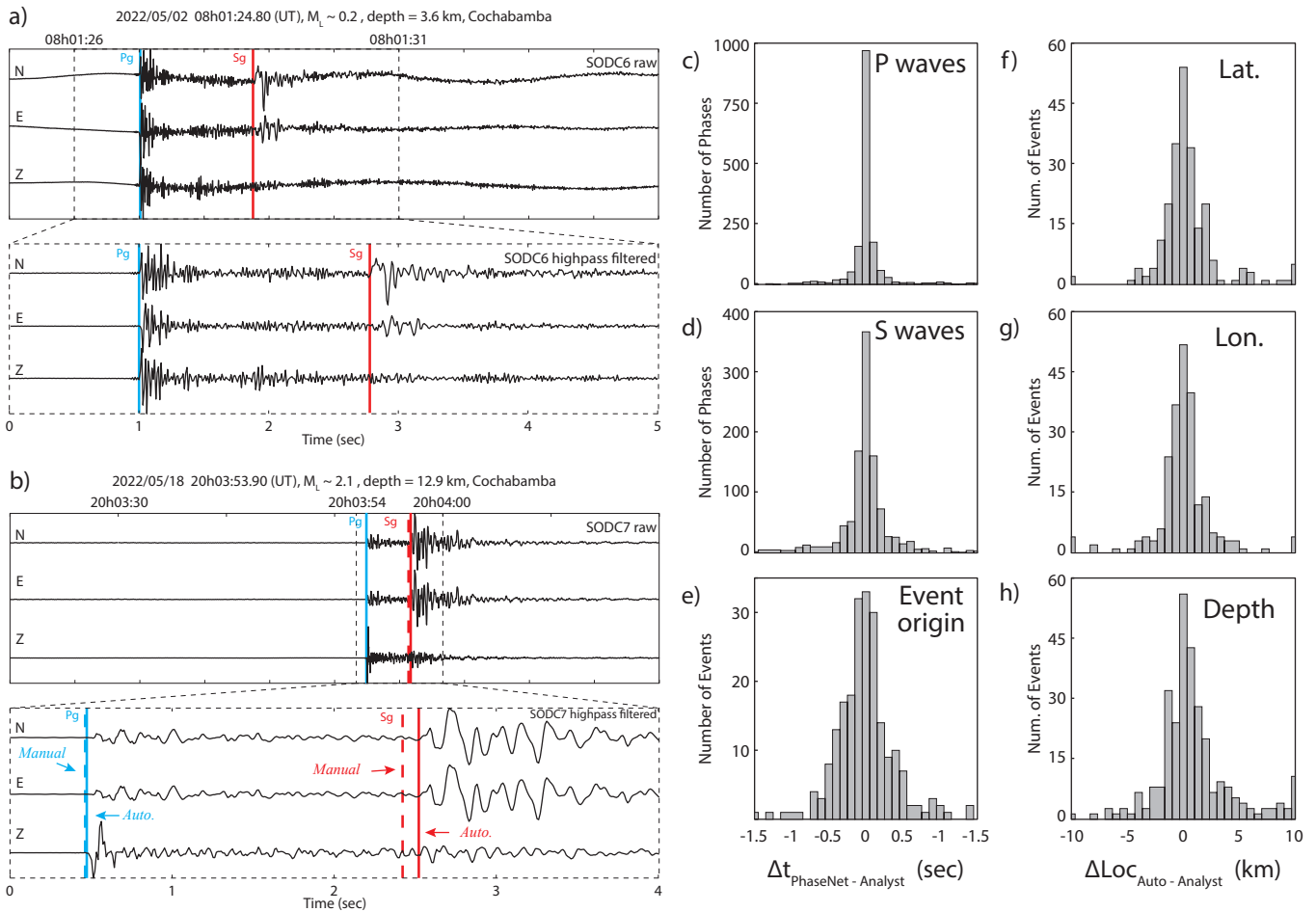


**Figure 5** Results from the automatic picking and locations procedures. **(a)** Example of a small event ( $M_L \sim 0.2$ ) only detected and picked with the automatic PhaseNet method. **(b)** Example of a moderate event ( $M_L \sim 2.1$ ) detected and picked by both analysts and PhaseNet. **(c) to (e)** Histograms of the time differences between PhaseNet and reference analyst picks. **(f) to (h)** Histograms of the location differences between the PhaseNet+REAL and the manual analysts procedures.

corroborated by the histograms presented in Figure 5f-h, indicating that the majority of the hypocentral location differences between manual and automated methods are less than 2 km.

The magnitude was computed using the original Richter (1935) formula for Southern California, with improvements from Hutton and Boore (1987) values of the three constants associated to the formula, i.e. associated to the geometric spreading, the attenuation and a correction. To obtain the  $M_L$  magnitude, a simulation of the Wood-Anderson seismometer was applied to the multicomponent signal. These traces are then filtered using a 2 Hz high-pass 2-pole Butterworth filter. The equation used for the magnitude calculation is:

$$M_L = \log_{10}(\text{Amp}) + 1.11 \log_{10}(\text{dist}) + 0.00189 * \text{dist} - 2.09 \tag{1}$$

Where  $\text{Amp}$  is the maximum amplitude in nm and  $\text{dist}$  (distance) in km.

### 3.2 Local uncertainties.

#### 3.2.1 Pick Precision

We present the precision, recall, and F1-score metrics for P and S phases after phase association were computed for the two catalogs (manual and automatic). The

results for P-wave picks, the precision, recall, and F1-score values were 0.987, 0.995, and 0.991, respectively, while for S-wave picks, these values were 0.988, 0.991, and 0.990, respectively (Table S2). The evaluation also documented the number of true positives (NTP), false positives (NFP), and false negatives (NFN), which were 2550, 33, and 14 for P-wave picks, and 1700, 20, and 15 for S-wave picks. These metrics underline the robustness of the PhaseNet technique and its capability to achieve near-human performance in phase picking, further validating its use in seismic event detection and location workflows (refer to Figure S6).

#### 3.2.2 Testing the implications of the velocity model.

In order to estimate the implications of the velocity model, we first plotted the Wadati diagrams for each seismic station (Figure S3). With the exception of SODC8 and 7, the  $V_P/V_S$  ratio measured for every station is close to the 1.75 considered in the initial velocity model. Given the values and average distance between events and stations in our network ( $\sim 30$  km), it can be reasonably assumed that potential velocity model differences would likely result in location differences of less than 3 km.



**Figure 6** Depth estimation sensitivity test for “Chapare Norte” cluster. **(a)**. For 62 events of this cluster, the measured S-P delays at the closest station SODC7 are represented according to their epicentral distance and their catalog depth (colored dots). The theoretical S-P delays according to distance & depth (colored font) are estimated from the velocity model used in this study (with a VP/VS ratio around 1.75). New depth estimation can be estimated from the measured S-P delays on SODC7 only (filled black dots), when fixing the epicenter obtained from the localization procedure. The 2 vertical black lines represent the distance range where are located 68% (1 standard deviation) of the clustered events. Thick black contour line represents the depth estimated for the mean of the observed S-P delays, for each epicentral distance. Light black contour line are computed respectively for the mean of the observed S-P delays  $\pm$  one standard deviation. **(b)** Histograms of depth estimations for the original catalog depths (green) and for the depth estimations derived from SODC7 S-P delays (black). The measured SODC7 S-P delays clearly point to a cluster around 12-13km depth (In this velocity model, a shallower cluster, less than 10 km, is very unlikely: A cluster at 10 km depth would have to be located at more than 12 km, instead of 3-4km, from SODC7 to explain the observed S-P delays). **(c)** & **(d)** Same as **(a)** & **(b)** but for a different velocity model: with the same P-wave velocities, and layers, but with a different VP/VS ratio, at 1.69 (the ratio which is locally measured on the station SODC7). The measured SODC7 S-P delays are here in favor of a slightly deeper cluster, around 15 km.

Moreover, to ascertain potential additional biases coming from the 1D velocity model, we conducted the joint hypocenter, velocity model and station coefficient determination of VELEST (Kissling et al., 1994), and the Joint Hypocenter Determination (Pujol, 1992). In order to achieve this, a set of relatively well-constrained earthquakes was selected from the initial catalog of events. This dataset was then filtered to include only earthquakes exhibiting an azimuthal gap of less than 180 degrees. Following this preselection, a subset of 138 earthquakes was obtained. The velocity model based on Ryan et al. (2016), Table S3, was then injected into VELEST as an initial model.

The best model derived from VELEST, falls within

less than 10% of all models aforementioned (Table S3d). The P and S time corrections calculated for each station do not exceed  $\pm$  1.5 seconds. The seismic station that presents the largest delays is SODC8, around +1.5 s while the other seismic stations show negative values smaller than -1.3 s. The distribution of the delays are consistent with the first order geological variations, SODC8 being on the eastern flank of the orogen, above shallow unconsolidated sedimentary units overthrusting the Chaco basin, while the stations to the west of the network lay on higher velocities and thicker tectonic units. (Figures S4a to c).

The epicenter localization uncertainties depend mostly on the seismic network coverage (primary

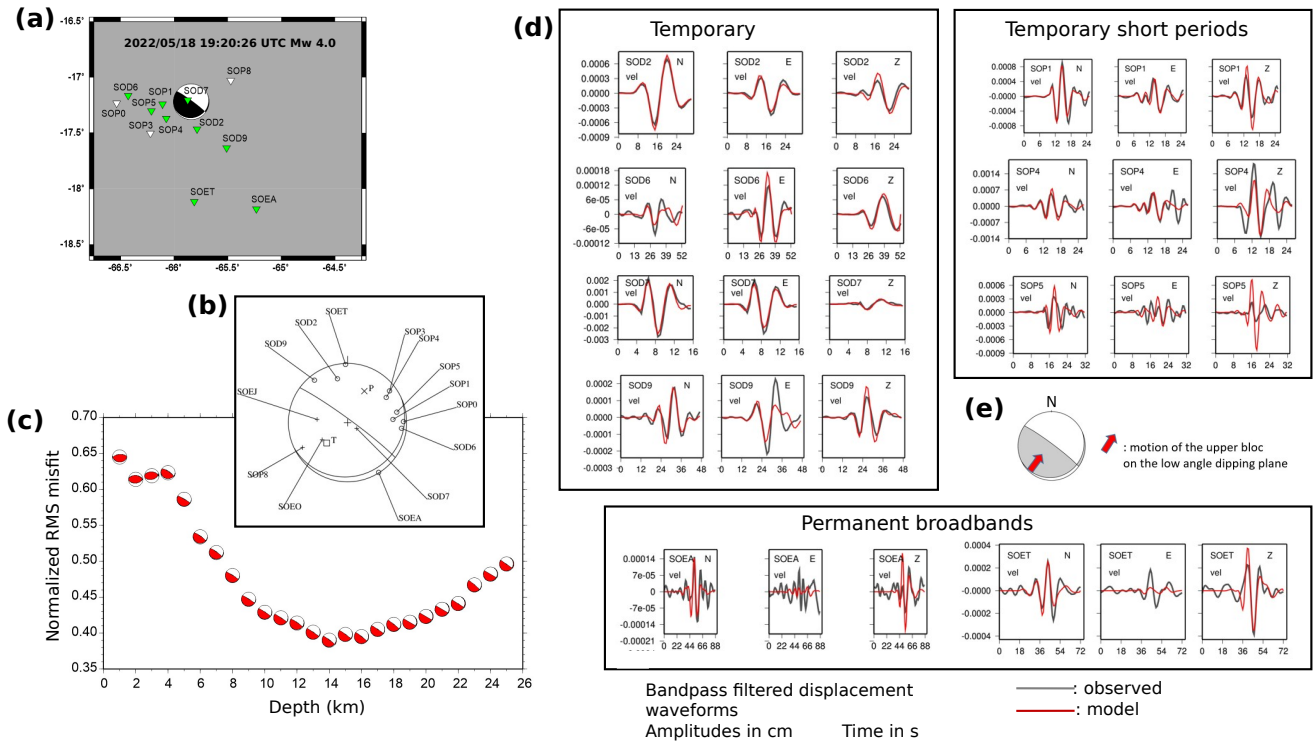


**Figure 7** FMNEAR waveform and polarity inversion of the 2022/05/18 19:20:26 UTC Mw 4.0 event. **(a)** Map showing seismic stations (triangles, in green for those whose waveforms are used) and the best focal mechanism found. **(b)** Polarities (+ for up, open circles for down), nodal planes, and P and T axes. **(c)** Exploration of the source depth. The best focal mechanism obtained for each depth value tested is plotted at the corresponding value of the normalized RMS misfit function. **(d)** Waveform fit of the bandpass filtered 3-component (N, E, Z) records in displacement, separated by network and/or sensor type. **(e)** Motion of the upper block (hanging wall) shown by the red arrow, assuming that the low angle dipping nodal plane is the fault plane. In the Figure, stations letter names are modified with respect to Figure 2 but numbers (0, 1, ...X) are the same.

and secondary azimuthal gaps, distance to the closest station, number of stations, Bondár et al., 2004), and are quite insensitive to velocity model errors (Laporte et al., 2024; Bondár et al., 2004; Bondár and Storck, 2011). The VELEST inversion provides horizontal uncertainties around 2-3 km, and can be considered significantly lower than 5km.

However, depth estimation is typically less well constrained. The accuracy of depth estimation is contingent upon the epicentral distance to the closest stations and the accuracy of the velocity model (e.g., Gomberg et al., 1990; Bondár et al., 2004; Bondár and Storck, 2011; Laporte et al., 2021; Letort et al., 2014; Hardebeck and Husen, 2010). Furthermore, the depth parameter may be subject to a trade-off with the estimation of the origin time during the localization procedure (e.g., Letort et al., 2014; Hardebeck and Husen, 2010).

In order to overcome the issue of the time origin and depth trade-off, it is possible to rely on observed S-P delays on nearby stations (e.g., Derode et al., 2023; Gomberg et al., 1990; Koirala et al., 2023). For the “Chapare Norte” cluster (May 18, 2022), 62 pairs of P & S arrivals are picked on SODC7, the closest station, located at less than 5km from the cluster, all with very similar S-P delays (2 +/- 0.1 seconds). These S-P delays depend on the epicentral distances, on the velocity model, and on the focal depth. First assuming the epicenters and the velocity model are correct, these S-P delays can there-

fore provide an estimation of the earthquake depths. Derived from S-P delays, the average cluster depth is thus found at 13.2 +/- 1 km (Figure 6a - b), close to the average original catalog depth (12.5 km).

The VP/VS ratio used for this study is around 1.75, but locally, around SODC7, this value is lower, around 1.69, estimated from the Wadati diagram (Figure S3). On the basis of this local VP/VS ratio, with the same P-wave velocities, and assuming that the epicentral location is correct, the S-P delays are consistent with a deeper cluster at 14.9 +/- .1 km (Figure 6 c - d). Further analysis has been conducted, and the results are presented in the supplementary data material (Figure S5).

**3.3 Focal mechanisms**

We performed the first waveform inversions incorporating stations from the temporary network (POBnet), using the FMNEAR method (Delouis, 2014), this algorithm proved its efficiency in Andean and Mediterranean context and its ability to provide reliable information on small-to-moderate magnitude earthquakes when the event is recorded with adequate azimuthal coverage (e.g., Derode et al., 2019; Menager, 2023). In the present case we invert jointly the waveforms and the first motion data (P-wave polarities).

During the period of this study we recorded a  $M_L$  4.3 event that occurred on May 18, 2022 (19h20 UTC, 15h20 local time, epicenter -17.224°N and -65.843°E), hereafter

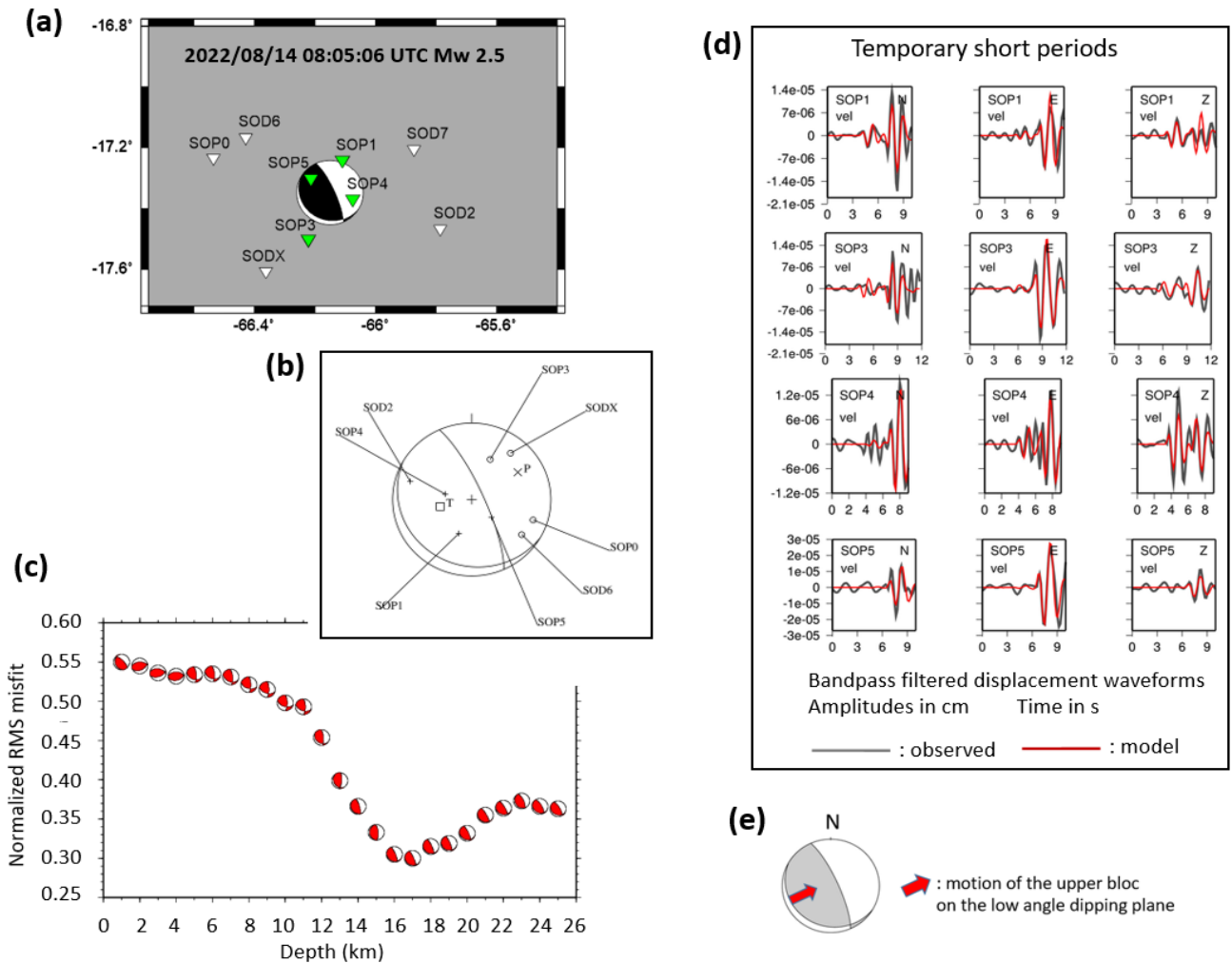


**Figure 8** Result of the joint inversion of first motion and waveform data for the 2022/08/14 08:05:06 UTC Mw 2.5 event, keeping only the four closest stations for the waveform part.

called “Chapare Norte”, and another of  $M_L$  2.8 on August 14, 2022 (08h05 UTC, epicenter  $-17.355^\circ N$  and  $-66.153^\circ E$ ), hereafter called “Cochabamba Centro”, both inside the temporary network.

The bandpass filter applied is adapted to each station and component but it is overall between 0.02 and 0.25 Hz for the broadband records and between 0.15 and 0.3 Hz for the short period records in the case of the largest  $M_L$  4.3 Chapare Norte event. In the case of the smaller  $M_L$  2.5 Cochabamba Centro event, the filtering domain lies between 0.35 and 1.0 Hz.

In both cases, the analysis of all the solutions tested by the nonlinear exploration of the source parameters, the quality of the modeling of the waveforms and the compatibility of the polarity data with the focal mechanism make it possible to establish that the solution is well constrained. The FMNEAR inversion results are synthesized in Figures 7 and 8.

For the “Chapare Norte” earthquake, the focal mechanism exhibits a low dipping nodal plane (strike  $65^\circ$ , dip  $10^\circ$ , rake  $29^\circ$ ) associated with a motion of the upper block (hanging wall) towards the NE (Figure 7e). From Figure 7c source depth can be considered as  $14 \pm 3$  km. The moment magnitude of the event is  $M_w$  4.0. The az-

imuth of a nodal plane becomes more difficult to determine when its dip is very low as is the case here. In any case, the focal mechanism can be described as a thrust towards NE on a sub-horizontal decollement.

The “Cochabamba Centro” earthquake exhibits a focal mechanism (strike  $120^\circ$ , dip  $15^\circ$ , rake  $55^\circ$ ) similar to the previous one. Given the low magnitude of the event, only the waveforms of the four nearest stations are used. From Figure 8c source depth can be considered as  $17 \pm 1$  km. The moment magnitude is  $M_w$  2.5. The reverse mechanism can be interpreted in a similar way as for the “Chapare Norte” earthquake, mostly coherent with another hanging wall thrusting to the NE of a decollement system that may be associated with a main system branch (further details in Figure 9).

For both earthquakes, the waveforms of the broadband and/or short-period stations could be modeled satisfactorily (Figures 7d and 8d), with a focal mechanism solution compatible with the first motion data. Additionally, the fact that the FMNEAR method is based on a non-linear exploration of the space of possible solutions allows us to calculate a confidence index measuring the uniqueness of the solution, ranging from 0 (highly non-unique) to 100% (unique) (Delouis, 2014). This confi-

dence index is higher than 87% for both events, indicating that their focal mechanisms are well constrained.

In supplementary material we show how the focal mechanism of the small Cochabamba Centro earthquake, unconstrained by polarities data alone (Figures S7 and S8), is correctly constrained by the joint inversion of polarities and waveforms (Figure S9).

### 3.4 Lateral variations of seismicity

In this study, we examine a seismic cluster that developed in the Corani-Chapare region at the foot of the mountain front (Figure 9), following the May 18, 2022 earthquake of  $M_L$  4.3 /  $M_w$  4.1 analyzed in the previous section. This seismic event was widely felt throughout the Cochabamba basin. Its effects were recorded from Sipesipe to Punata, as detailed in a macroseismic report by the Observatorio San Calixto (OSC), 2022. This earthquake is the largest earthquake recorded by the network in the period under review (as illustrated in Figure 4a). Furthermore, we observed a second cluster of seismic activity located less than 10 km from the village of Sipesipe. This village experienced substantial devastation due to an earthquake in 1909, situated at the western extremity of the Cochabamba basin (Vega, 1996).

The seismic activity spans the entire region, from Villa Tunari (SODC8 station) and the front of the thrust fault system in the east, to the western end of the Cochabamba basin (SODC0, SODC6 and SODC10 stations). While it impacts all tectonic units in the region, its effects are not uniform; specifically, the subandean and interandean tectonic zones belong to the Eastern Cordillera Forethrust Belt and the Eastern Cordillera Backthrust Belt. During the examined period, seismic activity was more concentrated near SODC10 and SODC7 stations, which are adjacent to the villages of Sipesipe and Corani-Chapare, and developed in clusters that were not seen before and which warrants further analysis.

### 3.5 Seismicity and its relation with structures at depth

Ryan et al. (2016) determined the Moho position beneath the region covered by the POB temporary network. As previously mentioned, the earthquakes recorded during the initial months of the experiment happened at midcrustal depths, primarily between 10 and 20 km. This places the hypocenters about 25-30 km above the Moho. Balanced structural cross-sections documented in the area show that seismicity occurs above the Brazilian shield basement, in the sedimentary cover detached and thrust over the basement. This sedimentary cover is made of several imbricated thrust sheets and numerous folds (Buford Parks and McQuarrie, 2019; McQuarrie, 2002).

In the studied area, the prevailing structural orientation of tectonic slivers and folds is predominantly NNW-SSE (N140-N150). The balanced cross-sections oriented NE-SW (approximately N050), as delineated by McQuarrie (2002) across the geological formations, indicate that the Chapare seismic cluster is situated near the basal

detachment of the thrust system, as illustrated in Figure 9. This discovery is particularly noteworthy considering that since the last significant study by Vega and Buforn (1991), there has been no tectonic interpretation provided for earthquakes of moderate magnitude in this region.

Whether the mainshock and its aftershocks are associated with the activation of the main structure or a thrust located less than 5 km higher in its hanging wall is uncertain, and falls either in the uncertainty of the hypocentral location or tectonic model. However, the shallowly dipping fault plane observed in the focal mechanism recorded on May 18th, 2022 (see Figure 7), aligns with the characteristics typically associated with decollement activation (e.g., Devlin et al., 2012). This seismicity could therefore be a consequence of the partial or full locking of this thrust segment, 50 km downdip the frontal fault system, and therefore the partial or full unlocking of the thrust system updip during large earthquakes.

The seismic cluster located west of Cochabamba, near Sipesipe, lies at a slightly shallower depth. It develops within or on the margin of a more internal tectonic sliver. It could be associated either with (1) the activation of a fault segment on the contact of the main internal sliver (in gray and white in Figure 9), (2) at the base of tectonic slivers affecting the sedimentary cover, in the Eastern Cordillera backthrust zone, or (3) with another fault parallel or oblique to the cross section trace and therefore not reported on the balanced cross section (such as a NW-SE strike-slip fault).

Seismic events below 10-15 km are scarce in the area, possibly due to a smaller seismogenic thickness compared to regions further east. However, earthquakes in this area are infrequent, with magnitudes below  $M_L$  2.0. These events are too small to determine focal mechanisms. The tectonic interpretation of this seismic cluster will therefore require additional data (with larger earthquakes for determining well-constrained focal mechanisms) and/or further effort using a larger set of methods (e.g. including double difference relocations).

The observed seismic activity distribution, when mapped onto the balanced cross-section, exhibits similarities to the seismic patterns found in the far western region of Nepal, at close distance from the Main Himalayan Thrust (Laporte et al., 2021; Hoste-Colomer et al., 2018). Within the confines of this principal thrust shear zone, a significant mid-crustal seismic cluster can be discerned at the downdip limit of the locked fault segment. Concurrently, additional seismic clusters emerge at the junctures between tectonic slivers. These slivers undergo either reactivation within the hanging wall of the Main Himalayan Thrust or experience fluid injections.

### 3.6 Discussion

The seismic stations of the POBnet experiment are located above the mid-crustal seismic clusters of the Cochabamba region within the Bolivian orocline to better resolve the relationship between regional seismicity

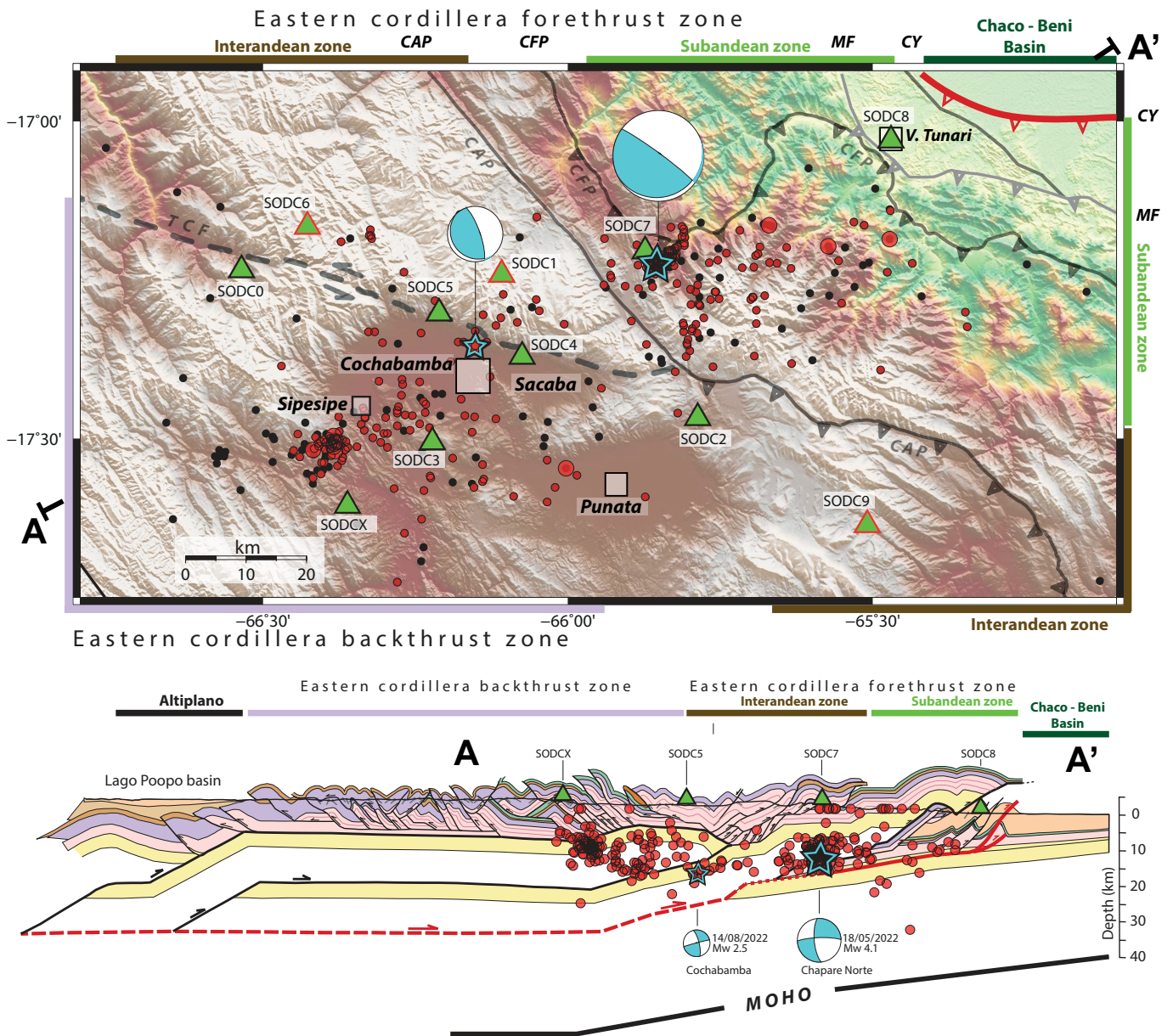


**Figure 9** May to October 2022 seismicity map and cross section. Moment tensor solutions in blue. Main active thrust system in red. (Top) Red circles and black dots respectively for high and low quality earthquakes (high quality associated with at least 4 P and 2 S phases with less than 250 degrees of gap). The large and small blue stars correspond to May 18<sup>th</sup> (ML 4.3 / Mw 4.1) and August 14<sup>th</sup> earthquake (ML 2.5 / Mw 2.5) respectively, the green triangles represent the seismic stations, and main populated villages are denoted by squares. (Bottom) The Balanced cross section from McQuarrie (2002) with seismicity projected on the section A to A'. TCF for Tunari Cochabamba Fault, CAP for Main Andean Thrust, CFP for Main Frontal Thrust, the surface trace of the most frontal thrust structure is represented in red (CY), MF for the Mandeyapecua Fault in gray line.

and geological structures. During the first six months of seismic monitoring in the Cochabamba region, 439 earthquakes with magnitudes exceeding  $M_L$  0.2 were detected and located (Figure 4a). The completeness magnitude of the resulting seismic catalog is approximately  $M_L$  0.9 (Figure 4b), illustrating the network’s ability to detect and locate very small earthquakes in the region. The hypocentral locations of these earthquakes are deemed reliable given the test we made with VELEST and S-P analysis sensibility, their relative uncertainties and the geometry of the instrumental network.

The results confirm the presence of mid-crustal clusters of earthquakes (located in the western and eastern part of POBnet), with most events occurring within the

first 20 km, amidst the basal decollement of the thrust system and the surface. This result suggests that the local earthquakes are much shallower than what was previously presented in the national catalog, in which a spread of earthquakes associated with a distribution of earthquakes within the first 50 km (Figure 2) is probably related to a trade-off between hypocentral depth and epicentral location due to the large distances and azimuthal gap associated with these earthquakes in the national bulletin (also shown in Figure 2). This provides further evidence in favor of continuing the experiment and ultimately establishing permanent stations in the region.

We interpret that part of this seismicity is a conse-

quence of the activity of the main thrust system, as previously suspected in southern Bolivia and in Argentina (e.g., Isacks, 1988; Brooks et al., 2011; Weiss et al., 2016; McFarland et al., 2017; Figueroa et al., 2020; Ammirati et al., 2022). This is confirmed by the focal mechanism of the largest shock recorded during the first 6 months of the experiment, a  $M_L$  4.3 that occurred on May 18th 2022. The hypocenters projected on the balanced cross section are close to the main thrust system or even shallower in its hanging wall. The earthquakes that occur in the hanging wall (e.g. in the vicinity of Sipesipe) appear to fall at the contact between tectonic slivers. However, note that strike-slip faults similar in orientation to the Cochabamba fault develop on both sides of the basin. They are not shown on the cross section as they are slightly oblique to it. Further documentation of this persistent cluster is therefore required to constrain its mechanism and to confirm the association of the seismicity at the contact between the mid-crustal duplex tectonic slivers (the largest earthquakes were too small for tying properly focal mechanisms).

Finally, evidence of reverse faulting activity is observed at mid-crustal depths, approximately 50 km from the surface trace of the most frontal thrusts beneath the toe of the high topography in the Chapare region (Figure 9). We interpret this cluster as indicative of the down-dip extension of a 50 km-large partially or fully locked fault segments of the main active thrust system. This distance is less than that of the fully locked fault zone proposed further south along the southern branch of the orocline on the basis of the GPS velocity field (Brooks et al., 2011; Weiss et al., 2016). In our region of interest, the Chapare cluster may be the result of persistent stress build-up at the downdip-end of a shorter locked fault zone, specific to the core of the orocline. Further monitoring is required to determine the permanence of this seismicity. Geodetic measurements are also needed to document the mechanical coupling between the two walls of the thrust in this region, which is probably capable of generating large earthquakes.

## Acknowledgements

The project was developed within the framework of the PhD work of the first author. It benefited from the long-lasting collaboration between CEA-DASE, France and OSC, Bolivia. We are grateful to all the Jesuit Societies in Bolivia, as well as to the OSC Directory, which allowed the first author to prepare a doctoral thesis. We are very grateful to the Gobernación of Cochabamba, especially to Dr. Fernando Fernandez (former head of the UGR) and his team for authorizing and facilitating the exchanges with the local communities while designing and maintaining the network. We are grateful to Stéphane Legarrec, head of DASE, and to François Schindelé, who facilitated the project; to Olivier Bresson and Fabrice Lepoint for their participation in the design and preparation of the experiment; to Nicolas Wendling-vazquez and Marine Laporte for early exchanges on the geophysical workflow and parameters. I sincerely express my heartfelt gratitude to the editor and reviewers for their valuable time, insightful feed-

back, and constructive opinions, which have greatly contributed to the improvement of this article.

## Data and code availability

Seismic catalog used in this research: <https://zenodo.org/doi/10.5281/zenodo.11205735>, last access on December 18, 2024.

The codes were elaborated with:

Python (<https://www.python.org/>),  
PyGMT (<https://www.pygmt.org/latest/>),  
GMT (<https://www.generic-mapping-tools.org/>),  
PhaseNet (<https://github.com/Al4EPS/PhaseNet>),  
REAL (<https://github.com/Dal-mzhang/REAL>),  
SEISAN (<https://seisan.info/>).

## Competing interests

All authors declare no conflict of interest.

## References

- Ammirati, J., Villaseñor, A., Chevrot, S., Easton, G., Lehujeur, M., Ruiz, S., and Flores, M. C. Automated Earthquake Detection and Local Travel Time Tomography in the South-Central Andes (32–35°S): Implications for Regional Tectonics. *Journal of Geophysical Research: Solid Earth*, 127(4), Apr. 2022. doi: 10.1029/2022jb024097.
- Ammirati, J.-B., Alvarado, P., and Beck, S. A lithospheric velocity model for the flat slab region of Argentina from joint inversion of Rayleigh wave phase velocity dispersion and teleseismic receiver functions. *Geophysical Journal International*, 202(1):224–241, Apr. 2015. doi: 10.1093/gji/ggv140.
- Baby, P., Hérail, G., Salinas, R., and Sempere, T. Geometry and kinematic evolution of passive roof duplexes deduced from cross section balancing: Example from the foreland thrust system of the southern Bolivian Subandean Zone. *Tectonics*, 11(3): 523–536, June 1992. doi: 10.1029/91tc03090.
- Beck, S., Barrientos, S., Kausel, E., and Reyes, M. Source characteristics of historic earthquakes along the central Chile subduction Askew et al zone. *Journal of South American Earth Sciences*, 11(2):115–129, Mar. 1998. doi: 10.1016/s0895-9811(98)00005-4.
- Bondár, I. and Storchak, D. Improved location procedures at the International Seismological Centre. *Geophysical Journal International*, 186(3):1220–1244, July 2011. doi: 10.1111/j.1365-246x.2011.05107.x.
- Bondár, I., Myers, S. C., Engdahl, E. R., and Bergman, E. A. Epicentre accuracy based on seismic network criteria. *Geophysical Journal International*, 156(3):483–496, Mar. 2004. doi: 10.1111/j.1365-246x.2004.02070.x.
- Bouchon, M. A simple method to calculate Green's functions for elastic layered media. *Bulletin of the Seismological Society of America*, 71(4):959–971, Aug. 1981. doi: 10.1785/bssa0710040959.
- Brooks, B. A., Bevis, M., Whipple, K., Ramon Arrowsmith, J., Foster, J., Zapata, T., Kendrick, E., Minaya, E., Echalar, A., Blanco, M., Euillades, P., Sandoval, M., and Smalley, R. J. Orogenic-wedge deformation and potential for great earthquakes in the central Andean backarc. *Nature Geoscience*, 4(6):380–383, May 2011. doi: 10.1038/ngeo1143.
- Buford Parks, V. M. and McQuarrie, N. Kinematic, flexural, and thermal modelling in the Central Andes: Unravelling age and signal

- of deformation, exhumation, and uplift. *Tectonophysics*, 766: 302–325, Sept. 2019. doi: 10.1016/j.tecto.2019.06.008.
- Campos, J., Hatzfeld, D., Madariaga, R., Lopez, G., Kausel, E., Zollo, A., Iannacone, G., Fromm, R., Barrientos, S., and Lyon-Caen, H. A seismological study of the 1835 seismic gap in south-central Chile. *Physics of the Earth and Planetary Interiors*, 132(1–3): 177–195, Sept. 2002. doi: 10.1016/s0031-9201(02)00051-1.
- Delouis, B. FMNEAR: Determination of Focal Mechanism and First Estimate of Rupture Directivity Using Near-Source Records and a Linear Distribution of Point Sources. *Bulletin of the Seismological Society of America*, 104(3):1479–1500, May 2014. doi: 10.1785/0120130151.
- Derode, B., Delouis, B., and Campos, J. Systematic Determination of Focal Mechanisms over a Wide Magnitude Range: Insights from the Real-Time FMNEAR Implementation in Chile from 2015 to 2017. *Seismological Research Letters*, 90(3):1285–1295, Mar. 2019. doi: 10.1785/0220180322.
- Derode, B., Gounon, A., Letort, J., Sylvander, M., Rigo, A., Benahmed, S., Grimaud, F., Latour, S., Pauchet, H., and Santamaria, A. Fluid-driven seismic swarms in the Gripp valley (Haute-Pyrénées, France). *Geophysical Journal International*, 234(3):1903–1915, Apr. 2023. doi: 10.1093/gji/ggad175.
- Devlin, S., Isacks, B. L., Pritchard, M. E., Barnhart, W. D., and Lohman, R. B. Depths and focal mechanisms of crustal earthquakes in the central Andes determined from teleseismic waveform analysis and InSAR. *Tectonics*, 31(2), Mar. 2012. doi: 10.1029/2011tc002914.
- Eichelberger, N. and McQuarrie, N. Kinematic reconstruction of the Bolivian orocline. *Geosphere*, 11(2):445–462, Apr. 2015. doi: 10.1130/ges01064.1.
- Fernandez, G. A., Assumpção, M., Nieto, M., Griffiths, T., and Convers, J. Focal mechanism of the 5.1Mw 2014 Lloja earthquake, Bolivia: Probing the transition between extensional stresses of the central Altiplano and compressional stresses of the sub-Andes. *Journal of South American Earth Sciences*, 91:102–107, Apr. 2019. doi: 10.1016/j.jsames.2019.01.001.
- Figueroa, S., Weiss, J. R., Hongn, F., Pingel, H., Escalante, L., Elías, L., Aranda-Viana, R. G., and Strecker, M. R. Late Pleistocene to Recent Deformation in the Thick-Skinned Fold-and-Thrust Belt of Northwestern Argentina (Central Calchaquí Valley, 26°S). *Tectonics*, 40(1), Dec. 2020. doi: 10.1029/2020tc006394.
- Funning, G. J., Barke, R. M., Lamb, S. H., Minaya, E., Parsons, B., and Wright, T. J. The 1998 Aiquile, Bolivia earthquake: A seismically active fault revealed with InSAR. *Earth and Planetary Science Letters*, 232(1–2):39–49, Mar. 2005. doi: 10.1016/j.epsl.2005.01.013.
- Glasgow, M., Schmandt, B., Wang, R., Zhang, M., Bilek, S. L., and Kiser, E. Raton Basin Induced Seismicity Is Hosted by Networks of Short Basement Faults and Mimics Tectonic Earthquake Statistics. *Journal of Geophysical Research: Solid Earth*, 126(11), Nov. 2021. doi: 10.1029/2021jb022839.
- Gomberg, J. S., Shedlock, K. M., and Roecker, S. W. The effect of S-wave arrival times on the accuracy of hypocenter estimation. *Bulletin of the Seismological Society of America*, 80(6A): 1605–1628, Dec. 1990. doi: 10.1785/bssa08006a1605.
- Hardebeck, J. and Husen, S. Earthquake location accuracy. 2010. doi: 10.5078/CORSSA-55815573.
- Havskov, J., Voss, P. H., and Ottemöller, L. Seismological Observatory Software: 30 Yr of SEISAN. *Seismological Research Letters*, 91(3):1846–1852, Mar. 2020. doi: 10.1785/0220190313.
- Hayes, G. P., Moore, G. L., Portner, D. E., Hearne, M., Flamme, H., Furtney, M., and Smoczyk, G. M. Slab2, a comprehensive subduction zone geometry model. *Science*, 362(6410):58–61, Oct. 2018. doi: 10.1126/science.aat4723.
- Hoste-Colomer, R., Bollinger, L., Lyon-Caen, H., Adhikari, L., Bailard, C., Benoit, A., Bhattarai, M., Gupta, R., Jacques, E., Kandel, T., Koirala, B., Letort, J., Maharjan, K., Matrau, R., Pandey, R., and Timsina, C. Lateral variations of the midcrustal seismicity in western Nepal: Seismotectonic implications. *Earth and Planetary Science Letters*, 504:115–125, Dec. 2018. doi: 10.1016/j.epsl.2018.09.041.
- Hutton, L. K. and Boore, D. M. The ML scale in Southern California. *Bulletin of the Seismological Society of America*, 77(6): 2074–2094, Dec. 1987. doi: 10.1785/bssa0770062074.
- Isacks, B. L. Uplift of the Central Andean Plateau and bending of the Bolivian Orocline. *Journal of Geophysical Research: Solid Earth*, 93(B4):3211–3231, Apr. 1988. doi: 10.1029/jb093ib04p03211.
- Jarrin, P., Nocquet, J.-M., Rolandone, F., Mora-Páez, H., Mothes, P., and Cisneros, D. Current motion and deformation of the Nazca Plate: new constraints from GPS measurements. *Geophysical Journal International*, 232(2):842–863, Sept. 2022. doi: 10.1093/gji/ggac353.
- Jiang, C., Fang, L., Fan, L., and Li, B. Comparison of the earthquake detection abilities of PhaseNet and EQTransformer with the Yangbi and Maduo earthquakes. *Earthquake Science*, 34(5): 425–435, Oct. 2021. doi: 10.29382/eqs-2021-0038.
- Jimenez, C., Tavera, H., Saavedra, M., and Calvo, M. El Terremoto de foco profundo de Bolivia 1994 a 8.2 Mw. *Revista de Investigación de Física*, 17(2):1–7, Dec. 2014. doi: 10.15381/rif.v17i2.11538.
- Kissling, E., Ellsworth, W. L., Eberhart-Phillips, D., and Kradolfer, U. Initial reference models in local earthquake tomography. *Journal of Geophysical Research: Solid Earth*, 99(B10):19635–19646, Oct. 1994. doi: 10.1029/93jb03138.
- Kley, J. Geologic and geometric constraints on a kinematic model of the Bolivian orocline. *Journal of South American Earth Sciences*, 12(2):221–235, Mar. 1999. doi: 10.1016/s0895-9811(99)00015-2.
- Koirala, B. P., Laporte, M., Bollinger, L., Batteux, D., Letort, J., Guilhem Trilla, A., Wendling-Vazquez, N., Bhattarai, M., Subedi, S., and Adhikari, L. B. Tectonic significance of the 2021 Lamjung, Nepal, mid-crustal seismic cluster. *Earth, Planets and Space*, 75(1), Oct. 2023. doi: 10.1186/s40623-023-01888-3.
- Lamb, S. Active deformation in the Bolivian Andes, South America. *Journal of Geophysical Research: Solid Earth*, 105(B11): 25627–25653, Nov. 2000. doi: 10.1029/2000jb900187.
- Laporte, M., Bollinger, L., Lyon-Caen, H., Hoste-Colomer, R., Duverger, C., Letort, J., Riesner, M., Koirala, B. P., Bhattarai, M., Kandel, T., Timsina, C., and Adhikari, L. B. Seismicity in far western Nepal reveals flats and ramps along the Main Himalayan Thrust. *Geophysical Journal International*, 226(3):1747–1763, Apr. 2021. doi: 10.1093/gji/ggab159.
- Laporte, M., Letort, J., Bertin, M., and Bollinger, L. Understanding earthquake location uncertainties using global sensitivity analysis framework. *Geophysical Journal International*, 237(2): 1048–1060, Mar. 2024. doi: 10.1093/gji/ggae093.
- Lavenu, A. Andean neotectonics between 1°N and 47°S (Ecuador, Bolivia and Chile): A review. *Revista De La Asociación Geológica Argentina*, 61(4):504–524, 2006.
- Lee, W. H. and Lahr, J. C. *HYP071: A Computer Program for Determining Hypocenter, Magnitude, and First Motion Pattern of Local Earthquakes*. 1975. doi: 10.3133/ofr75311.
- Letort, J., Vergoz, J., Guilbert, J., Cotton, F., Sebe, O., and Cano, Y. Moderate Earthquake Teleseismic Depth Estimations: New Methods and Use of the Comprehensive Nuclear-Test-Ban Treaty Organization Network Data. *Bulletin of the Seismological Society of America*, 104(2):593–607, Feb. 2014. doi: 10.1785/bssa0400020593.

- 10.1785/0120130126.
- Madariaga, R., Métois, M., Vigny, C., and Campos, J. Central Chile Finally Breaks. *Science*, 328(5975):181–182, Apr. 2010. doi: 10.1126/science.1189197.
- McBrearty, I. W. and Beroza, G. C. Earthquake Phase Association with Graph Neural Networks. *Bulletin of the Seismological Society of America*, 113(2):524–547, Jan. 2023. doi: 10.1785/0120220182.
- McFarland, P. K., Bennett, R. A., Alvarado, P., and DeCelles, P. G. Rapid Geodetic Shortening Across the Eastern Cordillera of NW Argentina Observed by the Puna-Andes GPS Array. *Journal of Geophysical Research: Solid Earth*, 122(10):8600–8623, Oct. 2017. doi: 10.1002/2017jb014739.
- McNamara, D. E. Ambient Noise Levels in the Continental United States. *Bulletin of the Seismological Society of America*, 94(4): 1517–1527, Aug. 2004. doi: 10.1785/012003001.
- McQuarrie, N. The kinematic history of the central Andean fold-thrust belt, Bolivia: Implications for building a high plateau. *Geological Society of America Bulletin*, 114(8):950–963, Aug. 2002. doi: 10.1130/0016-7606(2002)114<0950:tkhotc>2.0.co;2.
- Menager, M. Étude de l'utilisation de la méthode GRiD MT pour la détection et la caractérisation d'événements sismiques: De l'échelle régionale à l'échelle locale, 2023. <http://www.theses.fr/2023COAZ4012/document>.
- Mercier, J. L., Sebrier, M., Lavenue, A., Cabrera, J., Bellier, O., Dumont, J., and Machrare, J. Changes in the tectonic regime above a subduction zone of Andean Type: The Andes of Peru and Bolivia during the Pliocene-Pleistocene. *Journal of Geophysical Research: Solid Earth*, 97(B8):11945–11982, July 1992. doi: 10.1029/90jb02473.
- Nieto, M., Joly, B., Fernández M., G. A., Condori, F., Baldivieso, J., Griffiths, T., Arce, W., and Machaca, Z. Observatorio San Calixto – National Seismic, Infrasound and Strong Motion Network of Bolivia (Plurinational State of). *Summary of the Bulletin of the International Seismological Centre*, 55(II):29–49, Nov. 2021. doi: 10.31905/thgtn1jd.
- Pardo-Casas, F. and Molnar, P. Relative motion of the Nazca (Farallon) and South American plates since Late Cretaceous time. *Tectonics*, 6(3):233–248, 1987.
- Peterson, J. R. *Observations and modeling of seismic background noise*. 1993. doi: 10.3133/ofr93322.
- Pujol, J. Joint hypocentral location in media with lateral velocity variations and interpretation of the station corrections. *Physics of the Earth and Planetary Interiors*, 75(1–3):7–24, Dec. 1992. doi: 10.1016/0031-9201(92)90114-b.
- Retailleau, L., Saurel, J.-M., Laporte, M., Lavayssière, A., Ferrazzini, V., Zhu, W., Beroza, G. C., Satriano, C., Komorowski, J.-C., and Team, O. Automatic detection for a comprehensive view of Mayotte seismicity. *Comptes Rendus. Géoscience*, 354(S2):153–170, Jan. 2023. doi: 10.5802/crgeos.133.
- Richter, C. F. An instrumental earthquake magnitude scale\*. *Bulletin of the Seismological Society of America*, 25(1):1–32, Jan. 1935. doi: 10.1785/bssa0250010001.
- Rivadeneira-Vera, C., Assumpção, M., Minaya, E., Aliaga, P., and Avila, G. Determination of the fault plane and rupture size of the 2013 Santa Cruz earthquake, Bolivia, 5.2 Mw, by relative location of the aftershocks. *Journal of South American Earth Sciences*, 71:54–62, Nov. 2016. doi: 10.1016/j.jsames.2016.06.002.
- Ruiz, S., Klein, E., del Campo, F., Rivera, E., Poli, P., Métois, M., Christophe, V., Baez, J. C., Vargas, G., Leyton, F., Madariaga, R., and Fleitout, L. The Seismic Sequence of the 16 September 2015 Mw 8.3 Illapel, Chile, Earthquake. *Seismological Research Letters*, 87(4):789–799, May 2016. doi: 10.1785/0220150281.
- Ryan, J., Beck, S., Zandt, G., Wagner, L., Minaya, E., and Tavera, H. Central Andean crustal structure from receiver function analysis. *Tectonophysics*, 682:120–133, July 2016. doi: 10.1016/j.tecto.2016.04.048.
- Savvaadis, A., Young, B., Huang, G. D., and Lomax, A. TexNet: A Statewide Seismological Network in Texas. *Seismological Research Letters*, June 2019. doi: 10.1785/0220180350.
- Sempere, T., Hérail, G., Oller, J., and Bonhomme, M. G. Late Oligocene-early Miocene major tectonic crisis and related basins in Bolivia. *Geology*, 18(10):946, 1990. doi: 10.1130/0091-7613(1990)018<0946:loemmt>2.3.co;2.
- Silver, P. G., Beck, S. L., Wallace, T. C., Meade, C., Myers, S. C., James, D. E., and Kuehnel, R. Rupture Characteristics of the Deep Bolivian Earthquake of 9 June 1994 and the Mechanism of Deep-Focus Earthquakes. *Science*, 268(5207):69–73, Apr. 1995. doi: 10.1126/science.268.5207.69.
- Tan, Y. J., Waldhauser, F., Ellsworth, W. L., Zhang, M., Zhu, W., Michele, M., Chiaraluce, L., Beroza, G. C., and Segou, M. Machine-Learning-Based High-Resolution Earthquake Catalog Reveals How Complex Fault Structures Were Activated during the 2016–2017 Central Italy Sequence. *The Seismic Record*, 1(1): 11–19, Apr. 2021. doi: 10.1785/0320210001.
- Vega, A. and Buforn, E. Focal mechanisms of intraplate earthquakes in Bolivia, South America. *pure and applied geophysics*, 136(4):449–458, Dec. 1991. doi: 10.1007/bf00878581.
- Vega, B. Complementos a la historia sísmica de Bolivia, 1996.
- Venerdini, A., Alvarado, P., Ammirati, J.-B., Podesta, M., López, L., Fuentes, F., Linkimer, L., and Beck, S. Crustal seismicity in the Andean Precordillera of Argentina using seismic broadband data. *Tectonophysics*, 786:228450, July 2020. doi: 10.1016/j.tecto.2020.228450.
- Walter, J. I., Ogwari, P., Thiel, A., Ferrer, F., Woelfel, I., Chang, J. C., Darold, A. P., and Holland, A. A. The Oklahoma Geological Survey Statewide Seismic Network. *Seismological Research Letters*, 91(2A):611–621, Nov. 2019. doi: 10.1785/0220190211.
- Weiss, J. R., Brooks, B. A., Foster, J. H., Bevis, M., Echalar, A., Caccamise, D., Heck, J., Kendrick, E., Ahlgren, K., Raleigh, D., Smalley, R., and Vergani, G. Isolating active orogenic wedge deformation in the southern Subandes of Bolivia. *Journal of Geophysical Research: Solid Earth*, 121(8):6192–6218, Aug. 2016. doi: 10.1002/2016jb013145.
- Wiemer, S. and Wyss, M. Minimum Magnitude of Completeness in Earthquake Catalogs: Examples from Alaska, the Western United States, and Japan. *Bulletin of the Seismological Society of America*, 90(4):859–869, Aug. 2000. doi: 10.1785/0119990114.
- Zhan, Z., Kanamori, H., Tsai, V. C., Helmberger, D. V., and Wei, S. Rupture complexity of the 1994 Bolivia and 2013 Sea of Okhotsk deep earthquakes. *Earth and Planetary Science Letters*, 385: 89–96, Jan. 2014. doi: 10.1016/j.epsl.2013.10.028.
- Zhang, M., Ellsworth, W. L., and Beroza, G. C. Rapid Earthquake Association and Location. *Seismological Research Letters*, 90(6): 2276–2284, Sept. 2019. doi: 10.1785/0220190052.
- Zhang, M., Liu, M., Feng, T., Wang, R., and Zhu, W. LOC-FLOW: An End-to-End Machine Learning-Based High-Precision Earthquake Location Workflow. *Seismological Research Letters*, 93(5): 2426–2438, Mar. 2022. doi: 10.1785/0220220019.
- Zhu, W. and Beroza, G. C. PhaseNet: A Deep-Neural-Network-Based Seismic Arrival Time Picking Method. *Geophysical Journal International*, Oct. 2018. doi: 10.1093/gji/ggy423.
- Zhu, W., McBrearty, I. W., Mousavi, S. M., Ellsworth, W. L., and Beroza, G. C. Earthquake Phase Association Using a Bayesian Gaussian Mixture Model. *Journal of Geophysical Research: Solid Earth*, 127(5), May 2022. doi: 10.1029/2021jb023249.

The article *Unveiling midcrustal seismic activity at the front of the Bolivian altiplano, Cochabamba region* © 2025 by G.A. Fernandez is licensed under CC BY 4.0.